NPS-EC-95-008

NAVAL POSTGRADUATE SCHOOL
Monterey, California

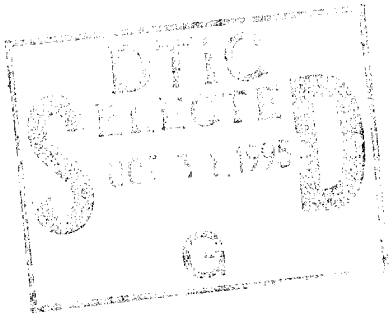

A RIGOROUS WAY OF INCORPORATING SEA SURFACE ROUGHNESS INTO THE PARABOLIC EQUATION

by

Ramakrishna Janaswamy

September 1995

This work was supported by the Navy/ASEE Summer Faculty Research Program and was conducted at the Tropospheric Propagation Branch, Division 543, NRaD, San Diego, CA.

Naval Postgraduate School
Monterey, California 93943-5000

Rear Admiral M.J. Evans
Superintendent

R. Elster
Provost

This work was supported by the Navy/ASEE Summer Faculty Research Program and was conducted at the Tropospheric Propagation Branch, Division 543, NRaD, San Diego, CA.

Approved for public release; distribution unlimited.

This report was prepared by:

R. Janaswamy

RAMAKRISHNA JANASWAMY
Associate Professor,
Department of Electrical and
Computer Engineering

Reviewed by:

M.A. Morgan

MICHAEL A. MORGAN
Chairman,
Department of Electrical and
Computer Engineering

Released by:

P.J. Marto

PAUL J. MARTO
Dean of Research

REPORT DOCUMENTATION PAGE

Form Approved
OMB No. 0704-0188

1. AGENCY USE ONLY (Leave blank)	2. REPORT DATE	3. REPORT TYPE AND DATES COVERED
		Jul 10–Sep 14, 1995

4. TITLE AND SUBTITLE
A Rigorous Way of Incorporating Sea Surface Roughness into the Parabolic Equation

5. FUNDING NUMBERS

6. AUTHOR(S)
Ramakrishna Janaswamy

7. PERFORMING ORGANIZATION NAME(S) AND ADDRESS(ES)
Naval Postgraduate School
Monterey, CA 93943-5000

8. PERFORMING ORGANIZATION REPORT NUMBER
NPSEC-95-008

9. SPONSORING / MONITORING AGENCY NAME(S) AND ADDRESS(ES)
Navy/ASEE Summer Faculty Research Program

10. SPONSORING / MONITORING AGENCY REPORT NUMBER

11. SUPPLEMENTARY NOTES
The views expressed in this report are those of the authors and do not reflect the official policy or position of the Department of Defense or the United States Government.

12a. DISTRIBUTION / AVAILABILITY STATEMENT
Approved for public release; distribution unlimited.

12b. DISTRIBUTION CODE

13. ABSTRACT *(Maximum 200 words)*

A rigorous formulation of rough earth parabolic equation (PE) is given. The formulation is based on casting the governing transform equations in terms of incident and reflected plane waves and using the rough-surface reduction factor directly in the spectral domain. Solution is performed by the well known split-step algorithm. Inclusion of surface roughness into the PE in this manner requires a redefinition of the Fourier transform pair. Several examples are considered showing comparisons with waveguide and other models.

14. SUBJECT TERMS	15. NUMBER OF PAGES
radiowave propagation, parabolic equation, ocean surface roughness	35
	16. PRICE CODE

17. SECURITY CLASSIFICATION OF REPORT	18. SECURITY CLASSIFICATION OF THIS PAGE	19. SECURITY CLASSIFICATION OF ABSTRACT	20. LIMITATION OF ABSTRACT
UNCLASSIFIED	UNCLASSIFIED	UNCLASSIFIED	SAR

Abstract

A rigorous formulation of rough earth parabolic equation (PE) is given. The formulation is based on casting the governing transform equations in terms of incident and reflected plane waves and using the rough-surface reduction factor directly in the spectral domain. Solution is performed by the well known split-step algorithm. Inclusion of surface roughness into the PE in this manner requires a redefinition of the Fourier transform pair. Several examples are considered showing comparisons with waveguide and other methods.

Objective

Our research objective is to develop a rigorous method to incorporate sea-surface roughness into the parabolic equation modeling of radiowave propagation.

Introduction

The Parabolic Equation (PE) method has emerged as an extremely valuable method for assessing radiowave propagation in the lower atmosphere in the presence of ducts. Propagation loss can be easily estimated over very long ranges of the order of a few hundred kilometers for frequencies through Super High Frequency (SHF) band, and for antenna heights extending up to a few hundred meters. It is also possible to directly account for finite conductivity of the earth in the PE. Reference [1] discusses the basic idea and the various approximations involved in the development of the PE. Although there are many different ways of solving the PE [2], none seem to offer the computational advantages of the split-step algorithm, originally developed by Tappert [3], in terms of the large range steps allowable. One of the current unresolved issues is the incorporation of sea-surface roughness into the PE. Several attempts have been made in the past all of which rely on some kind of approximation or post-processing of data obtained by running the PE over smooth earth. Reference [4] discusses some of these methods in detail. In this report, we present a direct way of incorporating surface roughness into the PE. The idea behind our approach is to cast the governing transform equations in terms of incident and reflected plane waves, and then use the rough surface reduction factor available for plane waves [5] directly in the spectral domain. Of course this will nesseciate the modification of the Fourier transform pair, as we will show shortly.

Theory

1. Smooth Earth

The starting point for our formulation is the standard parabolic equation, given, for example, in [1]. Assuming an $e^{-i\omega t}$ time dependence, we consider the parabolic equation in a medium with parameters (ϵ, μ_0):

$$\frac{\partial^2 u}{\partial z^2}(x,z) + 2ik_0\frac{\partial u}{\partial x}(x,z) + 2k_0^2 M(x,z)u(x,z) = 0, \tag{1}$$

where $u(x,z) = \sqrt{r\sin\theta}E_\phi(r,\theta)$, for horizontal polarization and $u(x,z) = \sqrt{\frac{r\sin\theta}{\epsilon(r,\theta)}}H_\phi(r,\theta)$ for vertical polarization, (r,θ,ϕ) being the usual spherical coordinates. The coordinate system is chosen such that the source is located at $\theta = 0$ and $r = a_e + z_s$, where a_e is the radius of the earth and z_s is the height of the source relative to the surface of the earth. Furthermore, $k_0 = \omega\sqrt{\epsilon_0\mu_0}$ is the free-space wavenumber, x is the range axis, z is the height axis, and

$$M(x,z) = \left(n - 1 + \frac{z}{a_e}\right) \times 10^6$$

is the modified refractive index under earth-flattened approximations [1]. The quantity E_ϕ (H_ϕ) is the $\phi-$component of the electric (magnetic) field. The complex dielectric constant, $\epsilon_{\rm rc}$, of the earth is $\epsilon_{\rm rc} = \epsilon_r + i\sigma/\omega\epsilon_0$, where σ is its conductivity. The parabolic equation given in (1) is to be solved subject to the approximate boundary condition

$$\frac{\partial u}{\partial z}(x,0) + \alpha_0 u(x,0) = 0, \tag{2}$$

where $\alpha_0 = ik_0\sqrt{\epsilon_{\rm rc} - 1}$ for horizontal polarization, $\alpha_0 = ik_0\sqrt{\epsilon_{\rm rc} - 1}/\epsilon_{\rm rc}$ for vertical polarization. The above boundary condition is approximate because it is valid for highly conductive soil satisfying $|\epsilon_{\rm rc}| \gg 1$. If this condition is not met, equation (2) must be imposed seperately for each constituent plane wave comprising u with α_0 replaced by

$$\alpha = ik_0\cos\theta_i\left[\frac{1 - \Gamma(\epsilon_{\rm rc};\theta_i)}{1 + \Gamma(\epsilon_{\rm rc};\theta_i)}\right],$$

where Γ is the reflection coefficient for a plane wave striking the earth at an angle θ_i with the normal. The actual field, u, does not satisfy the simple condition dictated by (2).

To solve (1) subject the boundary condition (2), the following mixed Fourier transform pair is defined [1]:

$$\tilde{u}(x,p) = \mathcal{F}(u) = \int_0^\infty u(x,z)[\alpha_0 \sin pz - p\cos pz]\, dz \tag{3a}$$

$$u(x,z) = \mathcal{F}^{-1}(\tilde{u}) = \frac{2}{\pi}\int_0^\infty \tilde{u}(x,p)\frac{\alpha_0 \sin pz - p\cos pz}{\alpha_0^2 + p^2}\, dp + S(x)e^{-\alpha_0 z}, \tag{3b}$$

where the latter term in (3b) decays with height and range and is due to the surface wave propagating on a non-perfectly conducting earth. This term is usually ignored in the solution for frequencies > 10 MHz. In the visible range $-k_0 \le p \le k_0$, one may identify p with the vertical wavenumber $k_0 \sin\psi$, where ψ is the grazing angle with respect to horizontal taken positive for waves approaching the interface $z = 0$.

Using the above Fourier transform pair, the solution to (1) in the presence of a slowly varying duct can be written as

$$u(x,z) = e^{ik_0(x-x_0)10^{-6}\times M}\mathcal{F}^{-1}\left\{e^{-ip^2(x-x_0)/2k_0}\mathcal{F}[u(x_0,z)]\right\} \tag{4}$$

To appreciate the development of the rough earth case, we will first rewrite the above Fourier transform pair (ignoring the surface wave) in the following equivalent form:

$$\tilde{u}(x,p) = \mathcal{F}_s(u) = \int_0^\infty u(x,z)e^{ipz}\, dz + \frac{1}{\Gamma_s(p)}\int_0^\infty u(x,z)e^{-ipz}\, dz \tag{5a}$$

$$u(x,z) = \mathcal{F}_s^{-1}(\tilde{u}) = \frac{1}{2\pi}\int_0^\infty \tilde{u}(x,p)\left[e^{-ipz} + \Gamma_s(p)e^{ipz}\right]\, dp, \tag{5b}$$

where

$$\Gamma_s(p) = \frac{p + i\alpha_0}{p - i\alpha_0}, \quad p > 0$$

is the plane-wave reflection coefficient for smooth earth, and subscripts s denote smooth earth case. In this form, it is clear from looking at (5b) that the total field is comprised of an incident plane wave of spectral amplitude $\tilde{u}(x,p)$ traveling towards the interface $z = 0$ and a corresponding reflected plane wave of amplitude $\Gamma_s(p)\tilde{u}(x,p)$ traveling away

from the interface. Furthermore, the field u satisfies the required smooth earth boundary condition of (2). Although the expression given above for $\Gamma_s(p)$ makes physical sense only for $p > 0$, we may analytically continue it for $p < 0$ and use the same expression to define it for negative p. With this continuation, we see that $\Gamma_s(-p) = 1/\Gamma_s(p)$. A second equivalent form which is symmetric with respect to the reflection coefficient and which makes use of the extended definition of $\Gamma_s(p)$ can be written down as:

$$\tilde{u}(x,p) = \mathcal{F}_s(u) = \sqrt{\Gamma_s(p)} \int_0^\infty u(x,z) e^{ipz}\, dz - \frac{1}{\sqrt{\Gamma_s(p)}} \int_0^\infty u(x,z) e^{-ipz}\, dz \qquad (6a)$$

$$u(x,z) = \mathcal{F}_s^{-1}(\tilde{u}) = \frac{1}{2\pi} \int_{-\infty}^\infty \frac{\tilde{u}(x,p)}{\sqrt{\Gamma_s(p)}} e^{-ipz}\, dp. \qquad (6b)$$

Note that there are no approximations involved, and all the three forms of the Fourier transform pair are equivalent. Also note that the form in (6) is particularly useful in extending the PE methodology to rough surfaces. The transform $\tilde{u}$ is seen to be an odd function of the transform variable p.

2. Rough Earth

In the rough earth case, we simply replace the smooth earth spectral reflection coefficient $\Gamma_s(p)$ with the corresponding rough earth one in the inversion formula (6b). A forward transform formula consistent with this must be defined seperately. The rough surface reflection coefficient, $\Gamma_r(p)$, is taken as

$$\Gamma_r(p) = \rho_0(p;\sigma_h)\Gamma_s(p), \qquad (7)$$

where $\rho_0(p;\sigma_h)$ is the rough surface reduction factor defined by [5]

$$\rho_0(p;\sigma_h) = e^{-2p^2\sigma_h^2} I_0(2p^2\sigma_h^2), \qquad (8)$$

and σ_h (m) is the r.m.s. height deviation determined from wind speed, μ (m/s), by

$$\sigma_h = 0.0051\mu^2. \qquad (9)$$

In equation (8), $I_0(.)$ is the modified Bessel function of the first kind of order zero. A simpler form in terms of elementary functions has been recommended in CCIR Report 1008-1 [6]:

$$\rho_0(p;\sigma_h) \approx \frac{1}{\sqrt{3.2\chi - 2 + \sqrt{(3.2\chi)^2 - 7\chi + 9}}}, \tag{10}$$

where $\chi = 2p^2\sigma_h^2$. Figure 1 shows the comparison between the exact and the approximate ρ_0 as a function of χ. Excellent agreement seen between the two permits the use of the much simpler approximate form in actual numerical computations. The formula for ρ_0 makes physical sense only for $p > 0$. As in the smooth earth case, we will extend the domain of definition of ρ_0 to include $p < 0$. We define ρ_0 for negative p as

$$\rho_0(-p;\sigma_h) = \frac{1}{\rho_0(p;\sigma_h)}, \quad p > 0 \tag{11}$$

We will present the development below for the important practical case of horizontal polarization. Vertical polarization can be handled in a similar fashion. In the subsequent discussion, we will drop the term σ_h from the argument of $\rho_0(p;\sigma_h)$ and its presence will be implied. For ranges far exceeding the heights, the plane waves arrive at very shallow grazing angles and it is adequate to take $\Gamma_s(p) \approx -1$ for horizontal polarization. With this approximation, we use (6) to write the transform pair as

$$\tilde{u}(x,p) = \sqrt{\rho_0(p)} \int_0^\infty u(x,z)e^{ipz}\,dz - \frac{1}{\sqrt{\rho_0(p)}} \int_0^\infty u(x,z)e^{-ipz}\,dz + \tilde{w}(x,p) \tag{12a}$$

$$u(x,z) = \mathcal{F}_r^{-1}(\tilde{u}) = \frac{1}{2\pi} \int_{-\infty}^\infty \frac{\tilde{u}(x,p)}{\sqrt{\rho_0(p)}} e^{-ipz}\,dp. \tag{12b}$$

The additional function $\tilde{w}(x,p)$ must be included to make the pair defined in (12) consistent. Of course, it is not needed for smooth earth. Alternately, one may add a function $w(x,z)$ to (12b) and use (12a) without $\tilde{w}$. However, we prefer not to do this, because, in this case, the solution cannot be expressed in the convenient form of (4). The quantity $\tilde{w}(x,p)$ is determined by the requirement that $\mathcal{F}[\mathcal{F}^{-1}\tilde{u}] = \tilde{u}$. It can be obtained as

$$\tilde{w}(x,p) = \frac{-i}{2\pi} \int_0^\infty \tilde{u}(x,q)K(p,q)\,dq, \tag{13}$$

where the kernel $K(p,q) = K(q,p)$ is

$$K(p,q) = \frac{1}{\sqrt{\rho_0(p)\rho_0(q)}}\left[\frac{\rho_0(p)-\rho_0(q)}{p-q} + \frac{1-\rho_0(p)\rho_0(q)}{p+q}\right]. \tag{14}$$

For $p = q$, the kernel is

$$K(p,p) = \frac{1}{\rho_0(p)}\left[\rho_0'(p) + \frac{1-\rho_0^2(p)}{2p}\right].$$

Note that (12a) and (13) constitute a Fredholm integral equation of the second kind for the unknown $\tilde{u}$ in terms of the known function u. It can be solved by any one of the several techniques available. A simple technique to use is the method of successive approximation or the so called Neumann series approach. In this work, we only concentrate on some simple techniques which are not necessarily efficient computationally. Note that the field, u, does not satisfy the boundary condition $u(x,0) = 0$ as it will for the smooth earth case. However, this does not pose any conceptual or numerical problems. For smooth earth, $\rho_0 = 1$ and, consequently, $K \equiv 0$. Also, observe that both $\tilde{u}(x,p)$ and $\tilde{w}(x,p)$ are odd functions of p. We may rewrite $\tilde{w}(x,p)$ in (13) in an operator form as

$$\tilde{w}(x,p) = -i\mathcal{W}(\tilde{u}).$$

Denoting the identity operator by $\mathcal{I}$ and substituting in (12a), we arrive at the desired forward transform as

$$\tilde{u}(x,p) = \mathcal{F}_r(u) = (\mathcal{I}+i\mathcal{W})^{-1}\left[\sqrt{\rho_0(p)}\int_0^\infty u(x,z)e^{ipz}\,dz - \frac{1}{\sqrt{\rho_0(p)}}\int_0^\infty u(x,z)e^{-ipz}\,dz\right].$$

Defining the function $u_+(x,z)$ by

$$u_+(x,z) = \begin{cases} u(x,z) & z > 0 \\ 0 & z < 0 \end{cases}$$

and denoting its ordinary complex Fourier transform as $\tilde{u}_+$,

$$\tilde{u}_+(x,p) = \mathcal{F}_o(u) = \int_{-\infty}^{\infty} u_+(x,z)e^{ipz}\,dz,$$

we write the complete Fourier transform pair for rough surface and horizontal polarization as

$$\tilde{u}(x,p) = \mathcal{F}_r(u) = (\mathcal{I} + i\mathcal{W})^{-1}\left[\sqrt{\rho_0(p)}\tilde{u}_+(x,p) - \sqrt{\rho_0(-p)}\tilde{u}_+(x,-p)\right] \qquad (15a)$$

$$u(x,z) = \mathcal{F}_r^{-1}(\tilde{u}) = \mathcal{F}_o^{-1}\left[\frac{\tilde{u}(x,p)}{\sqrt{\rho_0(p)}}\right], \qquad (15b)$$

where $\mathcal{F}_o^{-1}$ is the ordinary complex Fourier inverse

$$\mathcal{F}_o^{-1}(\cdot) = \frac{1}{2\pi}\int_{-\infty}^{\infty}(\cdot)e^{-ipz}\,dp.$$

It remains to define the inverse operator $\mathcal{P} = (\mathcal{I} + i\mathcal{W})^{-1}$. In computing the ordinary Fourier transform pair, one would normally use an N-point FFT. Let us assume that the various quantities are bandlimited over $-p_{\max} \le p \le p_{\max}$, and that the transform is evaluated at $p = 0, \Delta p, 2\Delta p, \ldots, (N-1)\Delta p$. Positive wavenumbers occur at $p = \Delta p, 2\Delta p, \ldots, (\frac{N}{2} - 1)\Delta p$, while negative wavenumbers occur at $(\frac{N}{2} + 1)\Delta p, (\frac{N}{2} + 2)\Delta p, \ldots, (N-1)\Delta p$. The value $\frac{N}{2}\Delta p$ corresponds to both $+p_{\max}$ and $-p_{\max}$. Let us assume that $\tilde{u}(x, \pm p_{\max}) = 0$. This can always be achieved in practice by a suitable window in the transform domain. Since $\tilde{u}$ is an odd function of p, we also have $\tilde{u}(x,0) = 0$. The same is true of $\tilde{w}$. Consider the vectors $\overline{\tilde{u}} = [\tilde{u}(x,\Delta p), \tilde{u}(x,2\Delta p), \ldots, \tilde{u}(x, \overline{N/2-1}\Delta p)]^t$ and $\overline{\tilde{w}} = [\tilde{w}(x,\Delta p), \tilde{w}(x,2\Delta p), \ldots, \tilde{w}(x, \overline{N/2-1}\Delta p)]^t$. One may use trapezoidal rule to discretize the integral in (13) as

$$\tilde{w}(x, m\Delta p) \approx \frac{-i\Delta p}{2\pi}\sum_{n=1}^{N/2-1}\tilde{u}(x,n\Delta p)K(m\Delta p, n\Delta p).$$

This can be written in a matrix form as

$$\overline{\tilde{w}} = -i\overline{W}\cdot\overline{\tilde{u}},$$

where $\overline{W}$ of order $(N/2-1 \times N/2-1)$ is the discrete version of the continuous operator $\mathcal{W}$ with elements

$$\overline{W}_{mn} = \frac{\Delta p}{2\pi}K(m\Delta p, n\Delta p), \quad m,n = 1,\ldots,N/2-1.$$

The discrete form of the continuous operator, $\mathcal{P}$, is then $\overline{P} = (I + \overline{W})^{-1}$, which is a matrix of order $N/2 - 1 \times N/2 - 1$. Note that $\overline{W}$ is a full matrix and I is an identity matrix of size $(N/2 - 1 \times N/2 - 1)$. In actual computations, we use (15a) to compute $\tilde{u}$ for positive p and extend the function over all p using odd symmetry. The operator $\overline{P}$ then acts on the positive wavenumber part of the spectrum occuring within the square brackets of (15a). We give below approximations to $\overline{P}$ of increasing orders of complexity and accuracy:

$$\overline{P} = (I + i\overline{W})^{-1} \quad \text{(exact, } O(N^3)\text{)} \tag{16a}$$

$$\approx I \quad \text{(zeroth order, no additional operations)} \tag{16b}$$

$$\approx I - i\overline{W} \quad \text{(first order, } O(N)\text{)} \tag{16c}$$

$$\approx I - i\overline{W} - \overline{W}^2 \quad \text{(second order, } O(N^3)\text{)} \tag{16d}$$

$$\approx I - i0.6438055\overline{W} - 0.5936575\overline{W}^2 \quad \text{(least-square, second order, } O(N^3)\text{)} \tag{16e}$$

Note that the $\overline{P}$ operator need be computed only once using any one of the above approximations for a given value of wind speed. In subsequent range stepping (equation (15a)), except for the zeroth order approximation, inclusion of $\tilde{w}$ involves one additional multiplication of the matrix $\overline{P}$ with the vector $\overline{\tilde{u}}$ and is of order $O(N^2)$. Since an FFT is of order $N\ln(N)$, the final algorithm time for range stepping will be of order $O(N^2)$. Diagonalyzing $\overline{P}$ has the potential of reducing the matrix multiplication time to $O(N)$ and the overall algorithm time to $O(N\ln(N))$. This will be explored in the future.

3. Numerical Results

We validate our PE formulation first by running a few sample cases and comparing with results from literature. A Hanning window with sequence

$$h(n) = \begin{cases} 1 & 0 \le n \le \frac{3N}{8} \\ \sin^2 \frac{4n\pi}{N} & \frac{3N}{8} \le n \le \frac{N}{2} \end{cases}$$

is used both in the spatial and wavenumber domains. A mirror image of $h(n)$ about $n = 0$ is used for negative wavenumbers. Note that the Hanning window forces a gradual

rolloff to zero over the last quarter of the positive wavenumber spectrum. We label the present method as PEERS, which stands for Parabolic Equation Exact Rough Surface.

The first example we try is that of propagation in standard atmosphere with $M = 340 + 0.118z$, where the height z is in meters. The transmitter is at a height of $z_s = 30$ m, the frequency of operation = 3 GHz, the maximum angle $\theta_{\max}$ that determines $p_{\max}$ is 1.43^0 (= 25 mrad), maximum height including rolloff is $z_{\max} = 512$ m. The size of FFT is determined from $z_{\max}$ and $\theta_{\max}$ by

$$N \geq 2\frac{2z_{\max}\sin\theta_{\max}}{\lambda_0},$$

where λ_0 is the free-space wavelength. The height and wavenumber increments are calculated from Nyquist criterion as

$$\Delta z = \frac{2z_{\max}}{N}, \quad \text{and } \Delta p = \frac{2\pi}{N\Delta z}.$$

We choose the vertical increment $\Delta z = 2$ m and $N = 512$. The range step was chosen to be 200 m. Figure 2 shows propagation factor (excess signal over the free-space case) versus receiver height for at the horizontal range of 40 km. Propagation factor, PF in dB, is defined as

$$PF = 10\log(|u|^2 x\lambda_0),$$

where x is the horizontal distance from transmitter. A positive (negative) value of propagation factor implies gain (loss) with respect to propagation in free-space. Although a direct comparison is not shown here, the lobing pattern compares very well with that given in [1].

The next example we consider is that of propagation in a tri-linear duct specified by

$$M(z) = \begin{cases} 340 + 0.118z & 0 \leq z \leq 135 \\ 499.03 - 1.06z & 135 \leq z \leq 150 \\ 322.33 + 0.118z & z \geq 150. \end{cases},$$

where z is in meters. The frequency of operation is 3 GHz, transmitter height is 30 m, $\theta_{\max} = 1.43^0$, and $z_{\max} = 512$ m. We choose $N = 512, \Delta z = 2$ m, and $\Delta x = 200$ m.

Figure 3 shows propagation versus receiver height at a range of 40 km. Once again a favorable agreement with [1] was obtained.

The final example we consider for smooth earth is propagation over a strong evaporation duct. The frequency is 10 GHz and the transmitter height is at 25 m. Refractivity profile for the evaporation duct is given in Table 1. We use $z_{\max} = 150$ m, $\theta_{\max} = 1.43^0, \Delta z = 0.293$ m, $N = 1024$, and $\Delta x = 200$ m. Figure 4 shows a comparison of the numerical results with those obtained by the waveguide model (MLAYER) [7] for a receiver height of 25 m. An excellent agreement is seen between the two, thus validating our PE algorithm.

We now consider a wind-roughened sea surface for the evaporation duct shown in Table 1. The wind speed is 10 m/s, which corresponds to an r.m.s. sea height of 0.51 m according to (9). All other parameters remain the same as before. Figure 5 comparses the propagation factor versus range for smooth and rough seas. Clearly, roughness has resulted in the reduction of the specular component as evidenced by the decreased excursions of the signal in the interference region. Furthermore, the loss increases at larger ranges. Figure 6 shows the comparison of the present numerical results with those predicted by MLAYER. Figure 7 shows comparison with TEMPER developed by the authors of [1] to also include surface roughness. It is based on first running the PE on the smooth earth case and then estimating the grazing angles using one of the spectral estimation procedures. This grazing angles is reused back into the PE to modify the results for the rough-earth case. The comparison is fair with all the results being within 1.5–2 dB of one another.

The results shown in Figure 6 were computed using the exact operator $\overline{P}$ given in (16a). We will now show the effects of using other approximations for $\overline{P}$. In each case we will compare the numerical results generated by the approximate operator with those generated by the exact operator. Figure 8 shows the results with the zeroth order approximation, which is the crudest. Note the shift in far-out minimum relative to the exact solution and the overall disagreement between the two results. The accuracy can

be dramatically improved by using the first order approximation. In this case no matrix inversion is required. Figure 9 shows the results with the first order approximation. There is some disagreement for very long ranges. Overall, solution by the first order operator compares favorable with the solution generated by the exact operator. Figure 10 shows the results with the second order operator. It is seen that the results are almost coincident with the exact results. Although the computation of the exact and the second order operators are both of the same complexity (of order $O(N^3)$), the second order operator can be used when inversion of a full matrix is not desired.

The last example we consider is that of a 45.7 m surface duct with refractivity profile given by

$$M(z) = \begin{cases} 350 - 0.335z & 0 \leq z \leq 45.7 \\ 329.36 + 0.1164z & z > 45.7, \end{cases}$$

where z is one again in meters. This example was considered in [4]. The transmitter is at height of 25 m, the frequency of operation = 10 GHz, and the antenna is omnidirectional. Propagation factor is calculated at a range of 200 km for various receiver heights. Figure 11 shows the results for a wind speeds of 10 m/s and 20 m/s. In both cases the results are compared with MLAYER results. It is seen that the agreement with the latter is very good, thereby validating our approach.

Future Work

Our future work will try to remove any computational inefficiencies in our algorithm. One might formulate the problem in terms of one-sided sine and cosine transforms instead of the full complex transforms defined in this work. More efficient schemes for computing the inverse operator $\overline{P}$ are certainly worth pursuing. Diagonalizing the operator $\overline{P}$ is another are of further investigation. Extention to vertical polarization is straightforward and will be looked at in the future.

TABLE 1. REFRACTIVITY DATA FOR EVAPORATION DUCT

Height (m)	Refractivity (M units)
0.000	340.00
0.135	323.00
0.223	321.76
0.368	320.53
0.607	319.31
1.000	318.11
1.649	316.94
2.718	315.83
4.482	314.80
7.389	313.91
12.182	313.26
20.000	312.99
20.086	313.00
33.115	313.38
54.598	314.81
90.017	317.99
148.413	324.04
165.000	325.76
300.000	339.745

References

[1] J. R. Kuttler and G. D. Dockery, "Theoretical description of the parabolic approximation/Fourier split-step method of representing electromagnetic propagation in the troposphere," *Radio Science*, vol. 26, no. 2, pp. 381-393, March-April 1991.

[2] F. B. Jensen, W. A. Kuperman, M. B. Porter, and H. Schmidt, *Computational Ocean Acoustics*, Chapter 6, New York: AIP Press, 1994.

[3] F. D. Tappert, "The parabolic approximation method," in *Wave Propagation and Underwater Acoustics*, (Lecture notes in Physics), J. B. Keller and J. S. Papadakis, Eds., New York: Springer-Verlag, vol. 70, 1977.

[4] A. Barrios, "Rough surface models implemented within the split-step parabolic equation algorithm," NRaD Technical Document 2630, April 1994.

[5] A. R. Miller *et al.,* "New derivation for rough surface reflection coefficient and for the distribution of sea-wave elevations," *IEE Proc.*, vol. 131, no. 2, pp. 114-116, April 1984.

[6] Report 1008-1, "Reflections from the surface of the Earth," vol. V of Recommendations and Reports of the CCIR, XVIIth Planery Assembly, ITU, Geneva, 1990.

[7] R. Pappert, "Field strength and path loss in a multilayer tropospheric waveguide environment," NOSC Technical Note 1366, October 1984.

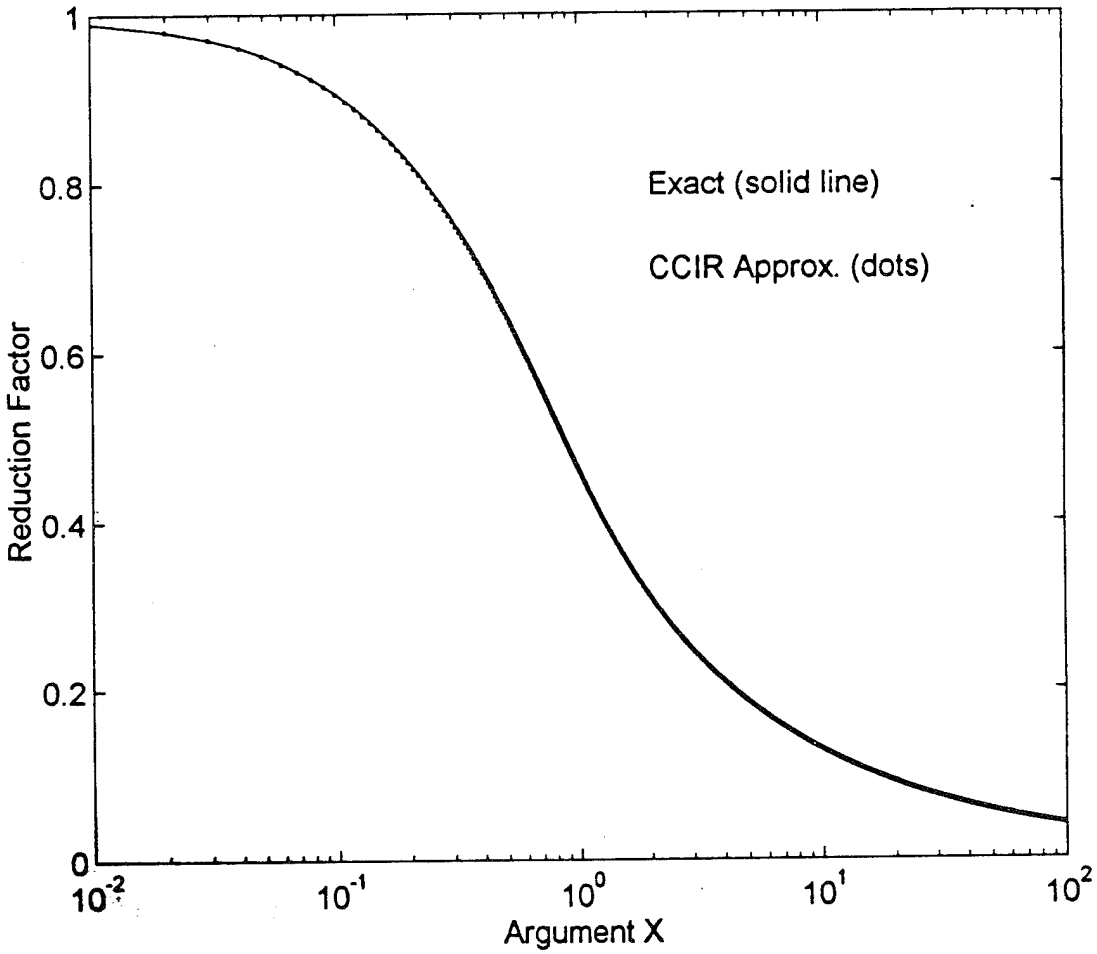

Figure 1. Exact and CCIR recommended formula for rough surface reduction factor ρ_0. The argument is $\chi = 2p^2\sigma_h^2$.

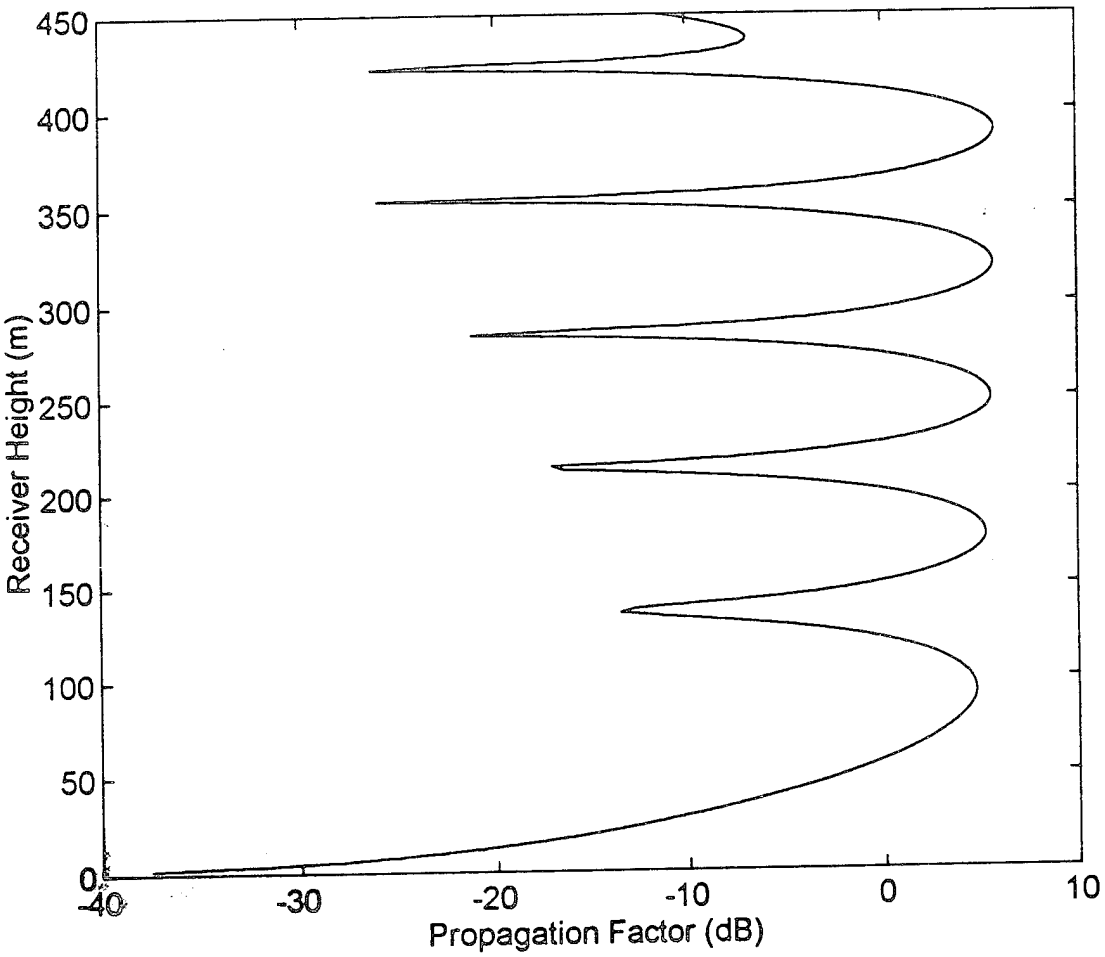

Figure 2. Propagation Factor versus receiver height at a range of 40 km in a standard atmosphere. Smooth earth, $z_s = 30$ m, $f = 3$ GHz, horizontal polarization and omnidirectional antenna.

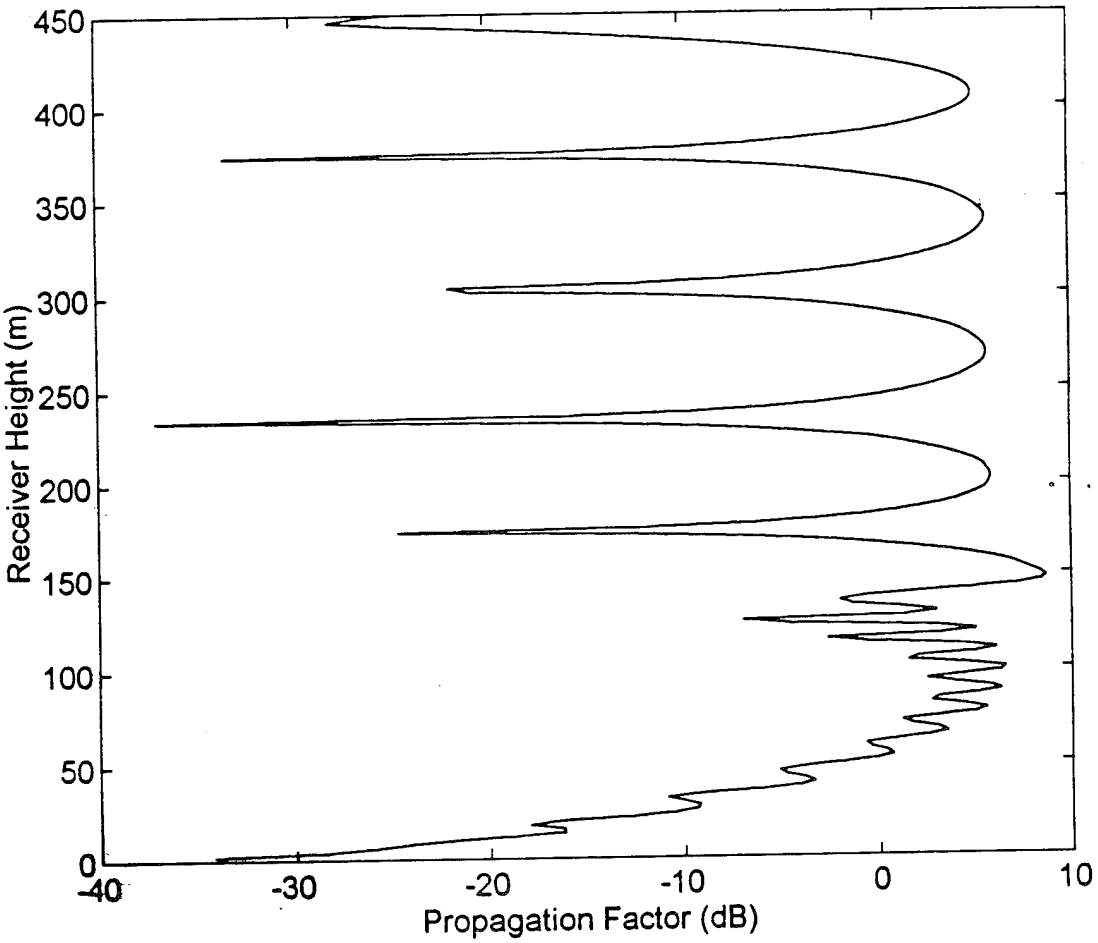

Figure 3. Propagation factor versus receiver height at a range of 40 km in a trilinear duct. Smooth earth, $z_s = 30$ m, $f = 3$ GHz, horizontal polarization and omnidirectional antenna.

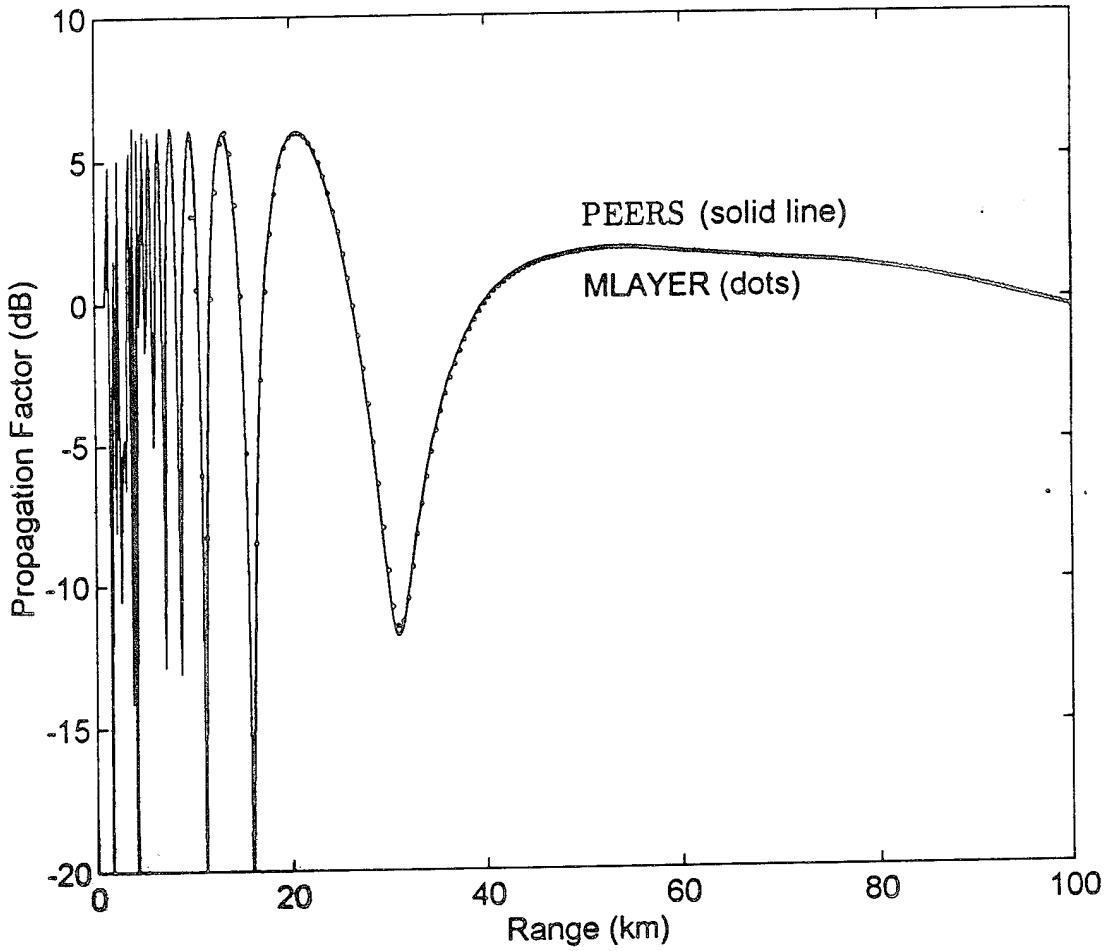

Figure 4. Propagation factor versus range at receiver height = 25 m in a 20 m evaporation duct. Smooth earth, $z_s = 25$ m, $f = 10$ GHz, horizontal polarization and omnidirectional antenna.

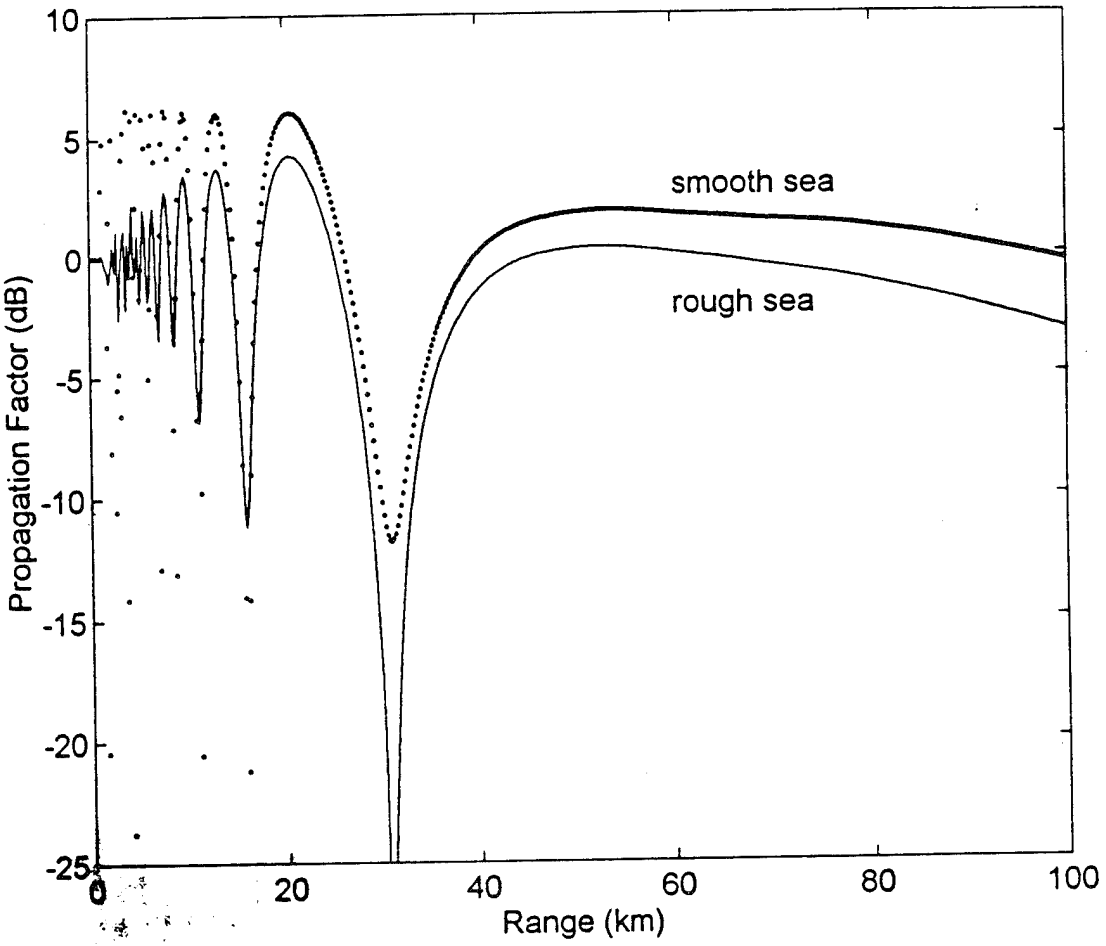

Figure 5. Propagation factor versus range at receiver height = 25 m in a 20 m evaporation duct. Smooth and rough sea (μ = 10 m/s), z_s = 25 m, f = 10 GHz, horizontal polarization and omnidirectional antenna.

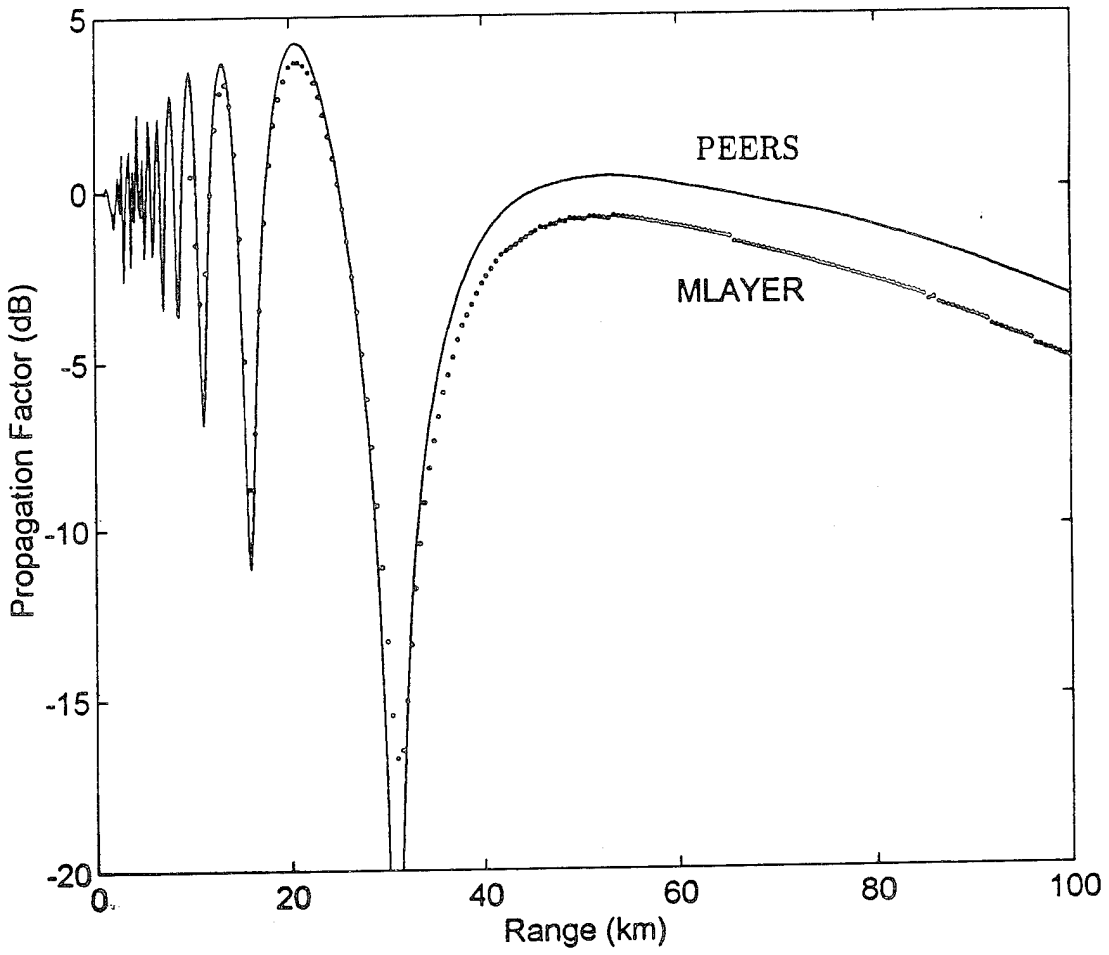

Figure 6. Comparison of propagation factor versus range at receiver height = 25 m in a 20 m evaporation duct. PEERS versus MLAYER, $z_s = 25$ m, $\mu = 10$ m/s, $f = 10$ GHz, horizontal polarization and omnidirectional antenna.

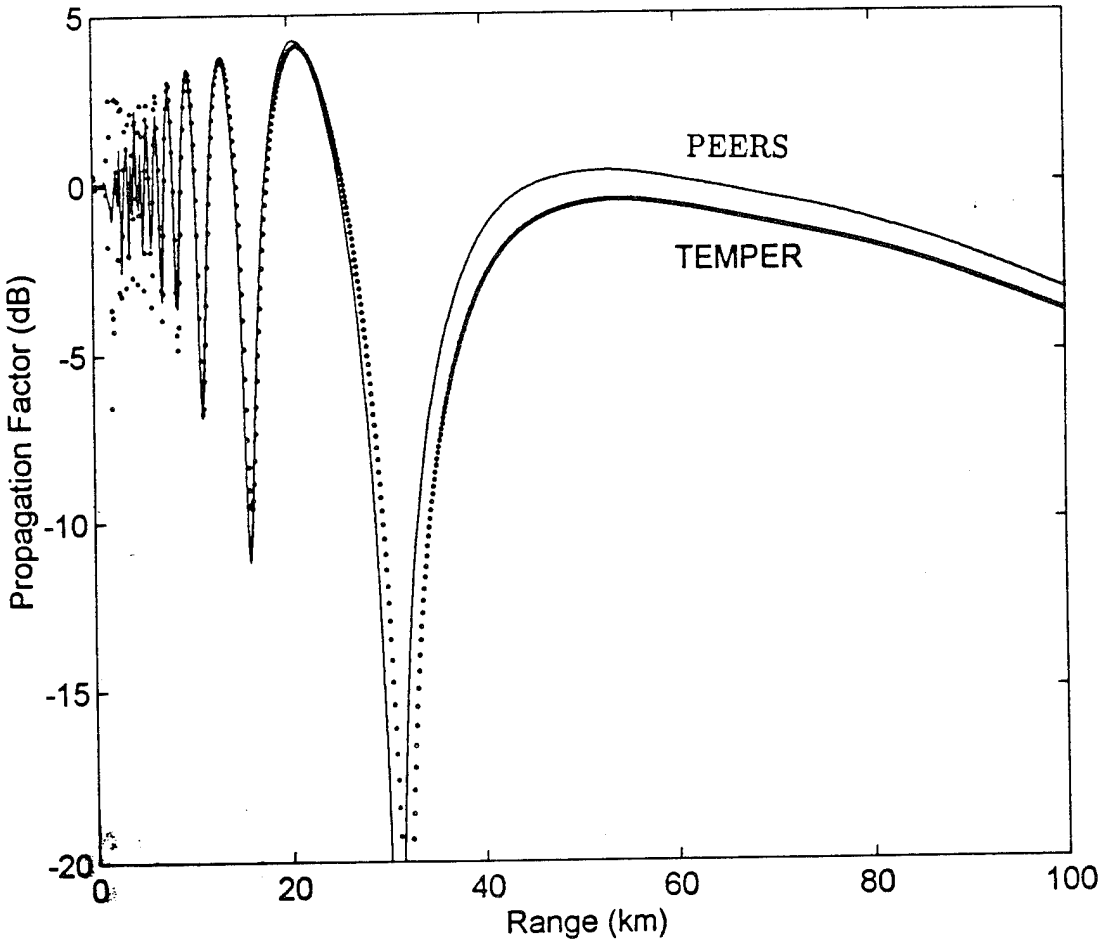

Figure 7. Comparison of propagation factor versus range at receiver height = 25 m in a 20 m evaporation duct. PEERS versus TEMPER, $z_s = 25$ m, $\mu = 10$ m/s, $f = 10$ GHz, horizontal polarization and omnidirectional antenna.

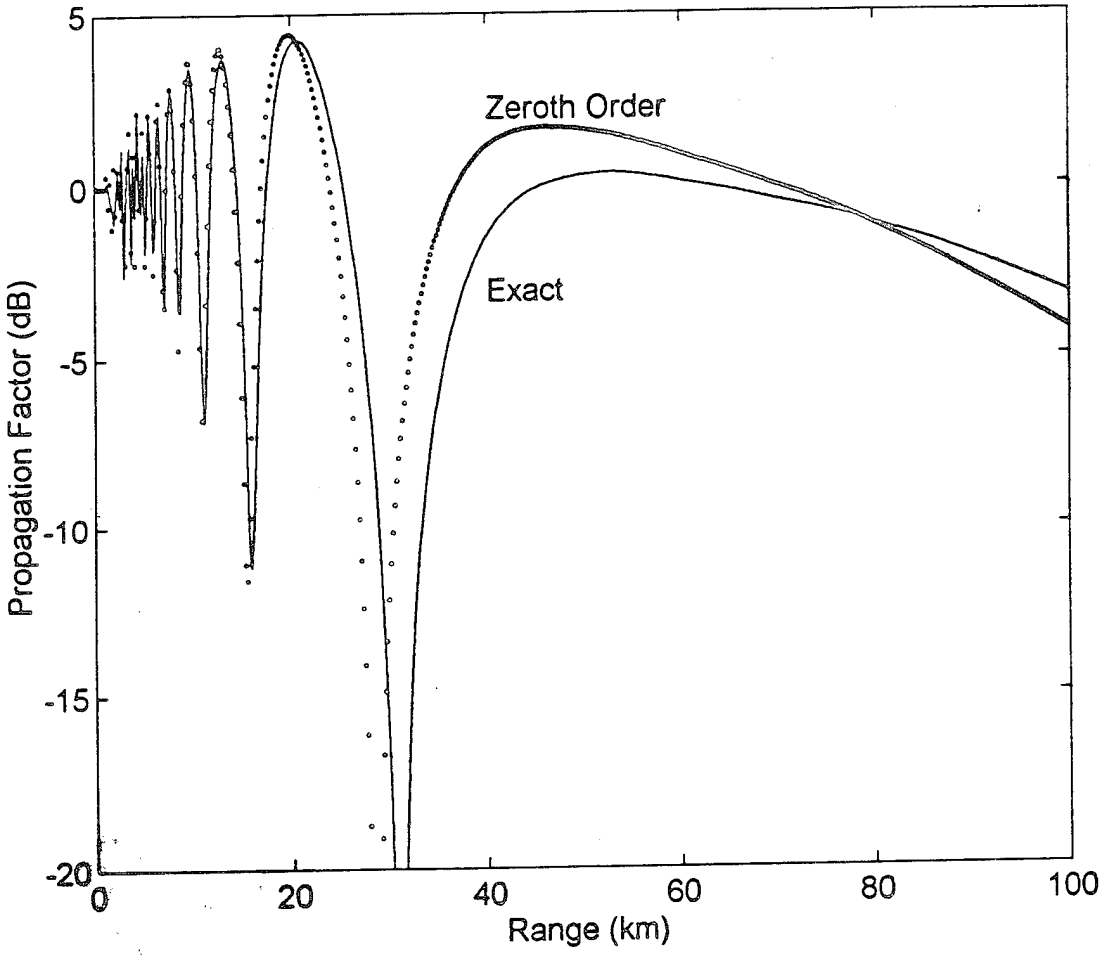

Figure 8. Comparison of propagation factor versus range at receiver height = 25 m in a 20 m evaporation duct by exact and zeroth order operators. $z_s = 25$ m, $\mu = 10$ m/s, $f = 10$ GHz, horizontal polarization and omnidirectional antenna.

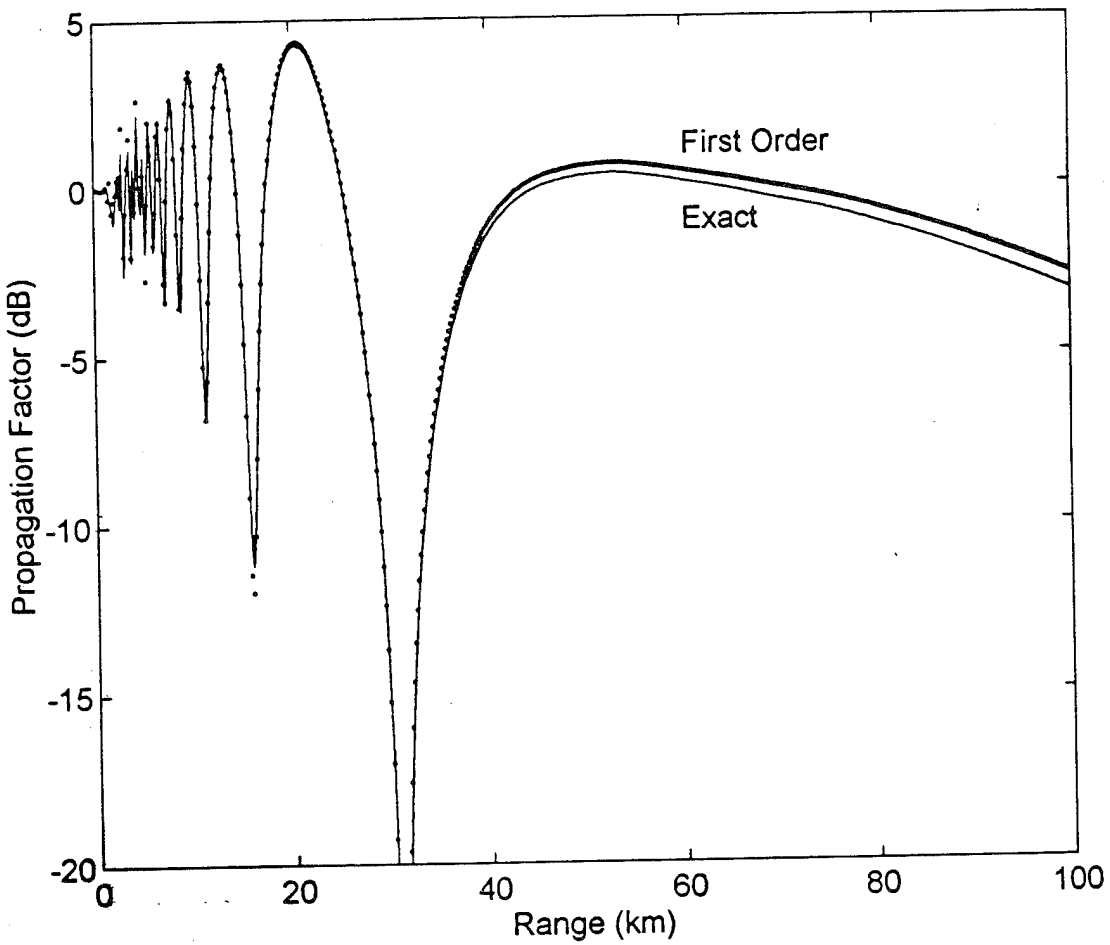

Figure 9. Comparison of propagation factor versus range at receiver height = 25 m in a 20 m evaporation duct by exact and first order operators. $z_s = 25$ m, $\mu = 10$ m/s, $f = 10$ GHz, horizontal polarization and omnidirectional antenna.

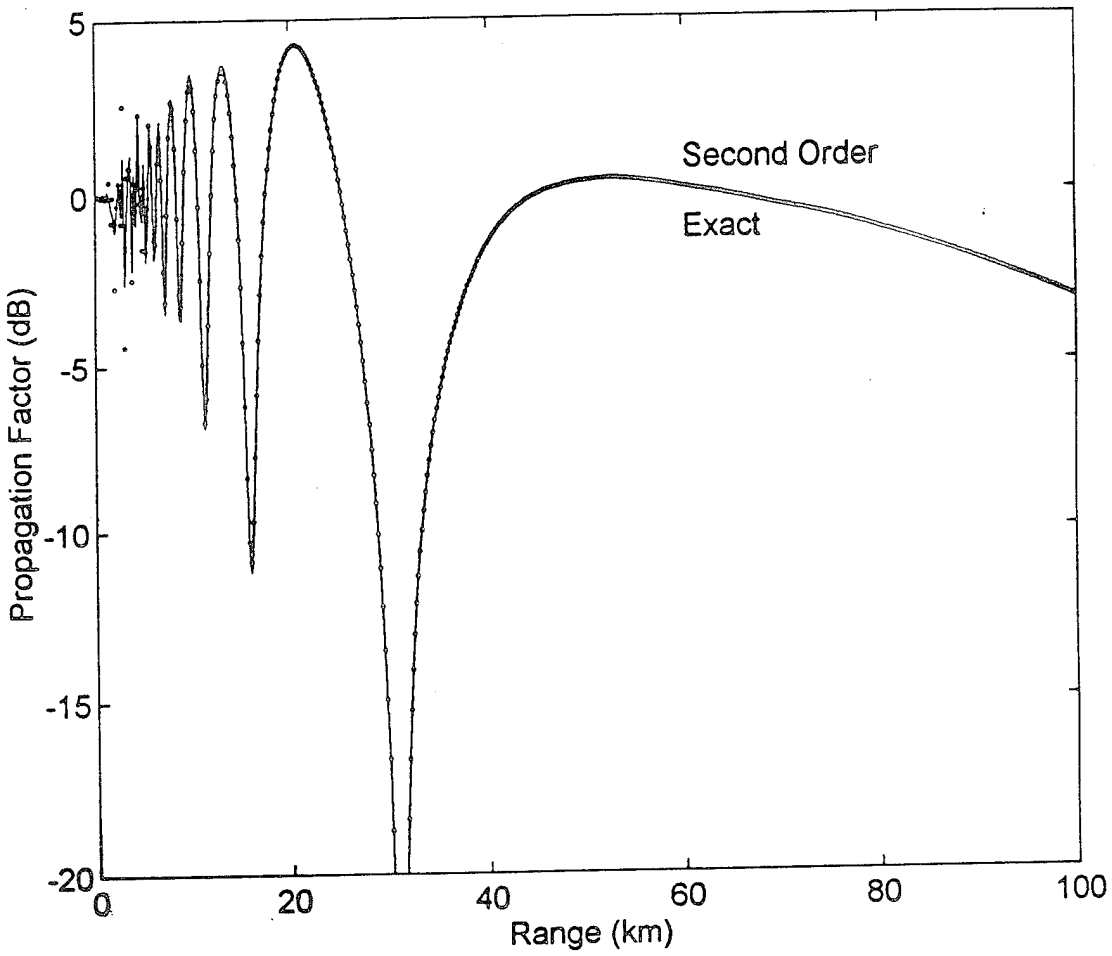

Figure 10. Comparison of propagation factor versus range at receiver height = 25 m in a 20 m evaporation duct by exact and secind order operators. z_s = 25 m, $\mu = 10$ m/s, $f = 10$ GHz, horizontal polarization and omnidirectional antenna.

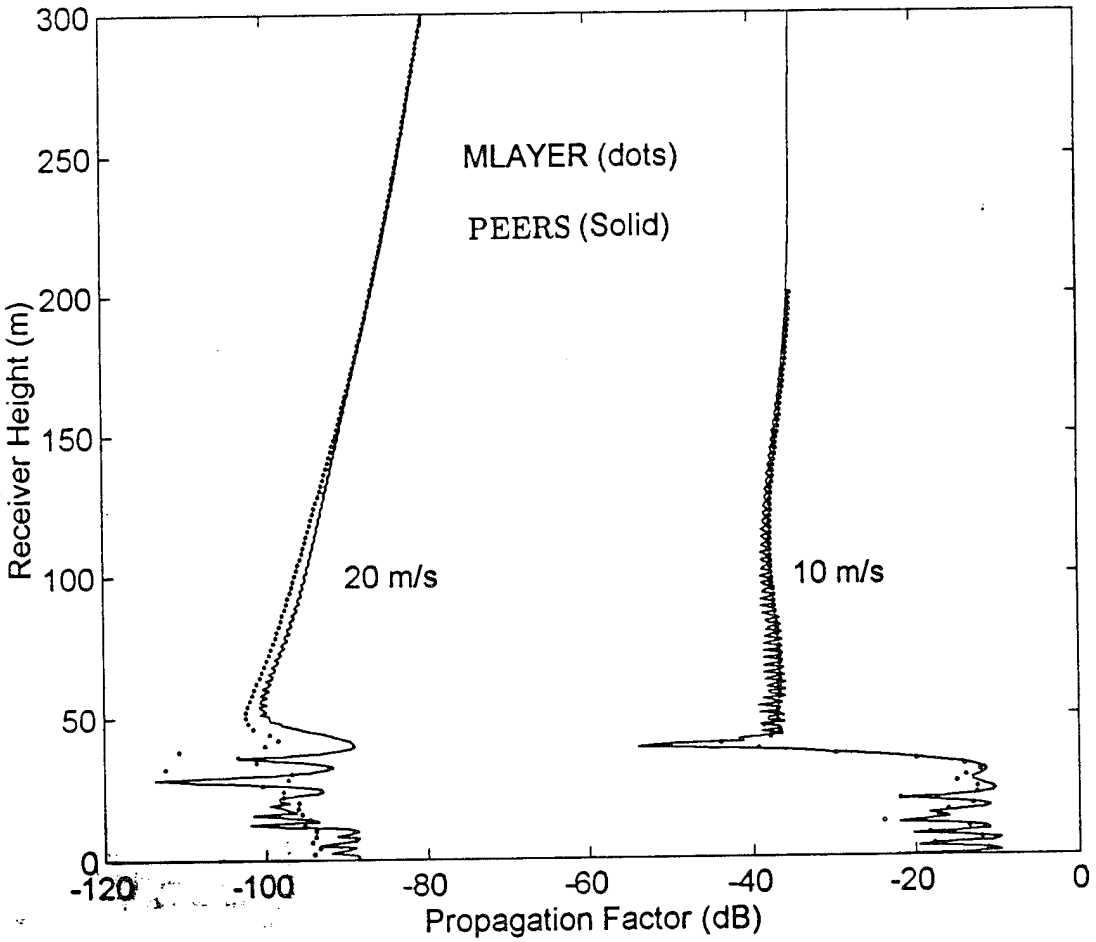

Figure 11. Propagation factor versus receiver height at range of 200 km in a 45.7 m surface duct. PEERS vs MLAYER, $z_s = 25$ m, $f = 10$ GHz, horizontal polarization and omnidirectional antenna.

INITIAL DISTRIBUTION LIST

		No. Copies
1.	Defense Technical Information Center Cameron Station Alexandria, VA 22304-6145	2
2.	Dudley Knox Library Code 52 Naval Postgraduate School Monterey, CA 93943-5101	2
3.	Chairman, Code EC Department of Electrical and Computer Engineering Naval Postgraduate School Monterey, CA 93943	1
4.	Dr. Ramakrishna Janaswamy, Code EC/Js Department of Electrical and Computer Engineering Naval Postgraduate School Monterey, CA 93943	10
5.	CDR Gus Lott, Code EC/Lt Department of Electrical and Computer Engineering Naval Postgraduate School Monterey, CA 93943	1
6.	Kenneth L. Davidson, Code MR/Ds Department of Meteorology 589 Dyer Road, Room 254 Naval Postgraduate School Monterey, CA 93943-5114	1
7.	Dr. Stephen Burk Naval Research Laboratory Marine Meteorology Division 7 Grace Hopper Avenue Monterey, CA 94943-5502	1
8.	Steven W. Payne Naval Research Laboratory Marine Meteorology Division 7 Grace Hopper Avenue Monterey, CA 93943-5502	1

9. William T. Thompson — 1
Naval Research Laboratory
Marine Meteorology Division
7 Grace Hopper Avenue
Monterey, CA 93943-5502

10. Mr. Kenneth Anderson — 1
NCCOSC RDTE DIV 543
53560 Hull Street
San Diego, CA 92152-5001

11. CDR H.G. Bancroft, III — 1
Deputy Chief, METOC Branch (SOJ3-OW)
HQ U.S. Special Operations Command
7701 Tampa Point Blvd.
MacDill AFB, FL 33621-5323

12. Ms. Amalia Barrios — 1
NCCOSC RDTE Division 543
53560 Hull St.
San Diego, CA 92152-5001

13. Tom Bell, Code 418200D (C2186) — 1
Naval Weapons Center
NAWCWPNS/CL
China Lake, CA 93555

14. David Boyer, Code N24 — 1
Naval Surface Warfare Center
Dahlgren Division
17320 Dahlgren Road
Dahlgren, VA 22448-5100

15. Charles B. Brooks, Code 5707 — 1
Naval Research Laboratory
4555 Overlook Avenue, SW
Washington DC 20375-5339

16. Clair Chua — 1
Naval Research Laboratory
Effectiveness of Naval Electronic
Warfare Systems
Washington DC 20375

18. Chris Diamond, Code N541 — 1
Naval Oceanographic Office
1002 Balch Blvd.
Stennis Space Center, MS 39522-5001

19. Dalcio K. Dacol, Code 7145 — 1
Naval Research Laboratory
Washington DC 20735-5350

20. Mr. Jean W. de Graff — 1
Naval Research Laboratory
4555 Overlook Avenue, SE
Washington DC 20375

21. L. Samuel Ditman, Code B42 — 1
Naval Surface Warfare Center, White Oak
10,901 New Hampshire Avenue
Silver Springs, MD 20903-5000

22. G. D. Dockery — 1
Applied Physics Laboratory
Johns Hopkins University
Laurel, MD 20707

23. Dr. Stephen Fast — 1
The Applied Research Laboratories
at the University of Texas-Austin
P.O. Box 8029
Austin, TX 78713-8029

24. Mr. Claude Hattan — 1
NCCOSC RDTE DIV 543
53560 Hull Street
San Diego, CA 92152-5001

25. Roger A. Helvey — 1
Naval Air Warfare Center Weapons Division
521 9th Street
Point Mugu, CA 93042-5001

26. Mr. Herbert Hitney — 1
NCCOSC RDTE DIV 543
53560 Hull Street
San Diego, CA 92152-5001

27. Guiseppe Izzi — 1
Naval Undersea Warfare Center Division
1176 Howell Street
Newport, RI 02841-1708

28. Phil Kerr — 1
DOD Joint Spectrum Center (JSC)
120 Worthington Basin
Annapolis, MD 21402-5064

29. CDR David G. Markham — 1
COMSPAWARSYSCOM (PMW 175)
Crystal Park 5, Suite 301
2451 Crystal Drive
Arlington, VA 22245-5200

30. Lee U. Martin, Code 5348 — 1
Naval Research Laboratory
Washington DC 20375-5320

31. William McIntrye — 1
Effectiveness of Naval Electronics
Warfare System (ENEWS)
Naval Research Laboratory
4555 Overlook Avenue, SW
Washington DC 20376

32. Denise M. Meanor — 1
Chief of Naval Operations (N096)
3450 Massachusetts Avenue, NW
U.S. Naval Observatory Bldg 1
Washington DC 20392-5421

33. Walter Dale Meyer — 1
HQ Air Weather Service/XOXT
102 West Losey Street, Room 105
Scott AFB, IL 62225-5206

34. LT David Milot — 1
NAVLANTMETOCCEN
9141 Third Avenue
Norfolk, VA 23511-2394

35. Eric L. Mokole, Code 5340 — 1
Naval Research Laboratory
4555 Overlook Avenue, SW
Washington DC 20375-5336

36. Mr. Richard Paulus — 1
NCCOSC RDTE DIV 543
53560 Hull Street
San Diego, CA 92152-5001

37. Mr. Wayne Patterson — 1
Office of Naval Research
ONR 322AM
800 North Quincy Street
Arlington, VA 22217-5660

38. Mary Peters, Code 7420 — 1
Naval Research Laboratory
4555 Overlook Avenue, SW
Washington DC 20375-5350

39. Timothy Politowicz, Code 8124 — 1
Naval Research Laboratory
4555 Overlook Avenue, SW
Washington DC 20375-5354

40. Dr. Juergen Richter — 1
NCCOSC RDTE DIV 54
53560 Hull Street
San Diego, CA 92152-5001

41. Mr. Ted Rogers — 1
NCCOSC RDTE DIV 543
53560 Hull Street
San Diego, CA 92152-5001

42. Jay S. Rosenthal — 1
Naval Air Warfare Center Weapons Division
521 9th Street
Point Mugu, CA 93042-5001

43. Frank Ryan 1
NCCOSC RDTE DIV
53560 Hull Street
San Diego, CA 92152-5001

44. S. N. Samaddar, Code 5340 1
Naval Research Laboratory
4555 Overlook Avenue, SW
Washington DC 20375-5336

45. Dr. William J. Stachnik 1
Office of Naval Research
800 North Quincy Street
Arlington, VA 22217-5660

46. Janet Stapleton 1
NSWC/DD Code F42
Dahlgren, VA 22448

47. Paul R. Tiedeman 1
PEO(USW)ASTO-E
2531 Jefferson Davis Highway
Arlington, VA 22242-5169

48. Dr. John Walters, Code 5330 1
Naval Research Laboratory
Washington DC 20375-5336

49. Thomas M. Willey 1
DOD Joint Spectrum Center
120 Worthington Basin
Annapolis, MD 21402-5064

50. Dave Williams, Code 61 1
Naval Undersea Warfare Center
Naval Undersea Warfare Center Detachment
New London, CT 06230

51. LCDR Zdenka S. Willis 1
COMNAVAIRSYSCOM (AIR-4.5M)
1421 Jefferson Davis Highway
Arlington, VA 22243-5120

52. LCDR James Zmyslo 1
Naval Information Warfare Activity
3801 Nebraska Avenue, NW
Washington DC 20393

53. Dr. K. H. Craig 1
Rutherford Appleton Laboratory
Chilton, Didcot
Oxfordshire 0X11 0QX
United Kingdom

54. Dr. Mireille F. Levy 1
Rutherford Appleton Laboratory
Chilton, Didcot
Oxfordshire 0X11 0QX
United Kingdom

55. Sherman Marcus 1
RAFAEL
Department 88
P.O. Box 2250
Haifa, Israel